Normal and Anomalous Codeposition of Ni-Co-Fe-Zn Alloys from EMIC/EG in the Presence of an External Magnetic Field

MEHDI EBADI, WAN J. BASIRUN, YATIMAH ALIAS, and MOHAMMAD R. MAHMOUDIAN

The codeposition of Ni-Co-Fe-Zn alloys from a mixture of 1-ethyl-3-methylimidazolium chloride (EMIC)/ethylene glycol (EG) was studied using potentiostatic electrodeposition in the potential range of –1.10 and –1.30 V *vs* saturated calomel electrode (SCE), using a permanent parallel magnetic field (PPMF) of 9 T. The uniform magnetic field was aligned parallel to the cathode surface. It was found that both normal and anomalous codeposition occurred. Films with different elemental percentage and deposit morphology were obtained from a mixture of EMIC/EG solution at the applied potentials (–1.10 and –1.30 V) in the absence and presence of a PPMF. The influence of magnetic field on the nucleation and growth process is studied with respect to the magneto-hydrodynamic effect (MHD) and applied potentials.

DOI: 10.1007/s11661-011-0605-3

I. INTRODUCTION

ALLOYS of the iron-group metal (Ni, Co, and Fe) have attracted interest because of their good physical properties. The alloys of the iron group (Ni, Co, and Fe) have higher corrosion resistance compared to their parent metals. In particular, the electrodeposition of iron group metals can exhibit anomalous deposition with the presence of Zn. Anomalous deposition occurs when the less noble metal (*i.e.*, Zn, Fe) deposit preferentially compared to more noble metals (*i.e.*, Ni, Co). Brenner[1] was among the first who identified the anomalous behavior of the Zn-iron group metals.

Several theories have been developed[2–4] to explain this anomalous phenomenon. Dahm and Caroll[5] attributed the anomalous behavior to the hydroxide suppression mechanism (HSM). Their theory suggests that the more noble ions are hindered from electrodeposition by the formation of the less noble metal hydroxides. This theory is based on the solubility constant (K_{sp}) of $M(OH)_2$ where the K_{sp} of Zn < Fe < Co < Ni.

In addition to the HSM theory, some authors[6–10] found that the under potential deposition (UPD) of less noble ions can also lead to anomalous electrodeposition. At lower potentials, normal codeposition takes place, whereas at higher potentials, anomalous codeposition occurs from aqueous solution.[11] Several research groups have been using ionic liquids in the metal finishing process[12–14] to find better conditions for metal electrodeposition. However, the high viscosity of ionic liquids remains the main obstacle compared to aqueous solutions.

The viscosity of ionic liquids is a function of temperature. Also, the conductivity of ionic liquids is strongly dependent on temperature, which obeys an Arrhenius-type behavior. The melting point of 1-ethyl-3-methylimidazolium chloride (EMIC) is 350 K to 352 K (77 °C to 79 °C), and the viscosity of EMIC decreases with the increase in temperature. Gou and Sun[15] have done electrodeposition of Ni and Ni-Zn alloys from EMIC ionic liquid solvent. It was found that the electrodeposition of Ni (II) occurs preferentially compared to the electrodeposition of Zn (II). The UPD of the Zn-Ni alloy was shifted to more negative potentials compared to pure Ni. Basically, the structure of Co (II), Ni (II), Fe (II), and Zn (II) in the EMIC can be illustrated in Figure 1.

Crystal structure shows that extended hydrogen bonding networks exist between $(MCl_4)^{2-}$ and ring hydrogen of EMIC. Furthermore, Koura *et al.*[16] attempted the electrodeposition of Ni-Zn from $NiCl_2$-$ZnCl_2$-EMIC-EtOH. They noticed that the addition of EtOH into the molten salts (EMIC) resulted in the improvement of current efficiency. The nucleation and growth mechanism of electrodeposition of transition metals in mixtures of ionic liquids became an interesting subject. Furthermore, the electrodeposition and morphologies of Ni coatings from ionic liquid based on choline chloride (ChCl) mixed with hydrogen bound donor such as ethylene glycol (EG) were also investigated.[17] In this study, EG was mixed with EMIC to reduce viscosity, hence improving the current efficiency for electrodeposition.

The application of a magnetic field during electrodeposition is already an established phenomenon. The presence of a magnetic field parallel (permanent parallel magnetic field (PPMF)) to the electrode surface or perpendicular to the direction of current increases the

MEHDI EBADI, Postdoctoral Researcher, WAN J. BASIRUN, Professor in Electrochemistry and Materials, Academic Staff, YATIMAH ALIAS, Professor in Electrochemistry, Academic Staff, and MOHAMMAD R. MAHMOUDIAN, Postdoctoral Student, are with the Department of Chemistry, Faculty of Science, University of Malaya, 50603 Kuala Lumpur, Malaysia. Contact e-mail: mehdi_2222002@yahoo.com

Manuscript submitted September 1, 2010.
Article published online January 27, 2011

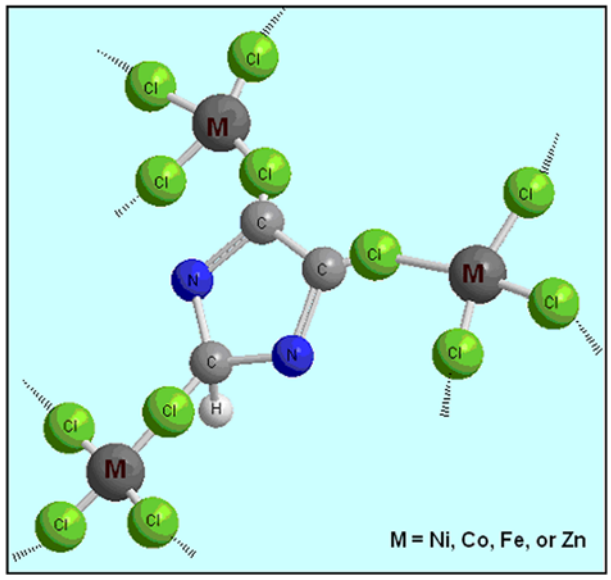

Fig. 1—Organic-inorganic complexation of EMIC-M in the solution phase.

mass transport to the electrode surface, and this is known as the magnetohydrodynamic (MHD) effect. The major force in the MHD effect is the Lorentz force, where it is the product of the current density and the magnetic field strength in perpendicular directions, or $(F_L) = J \times B$.

This study presents the influence of magnetic field and applied potentials on the quality (morphology and nucleation process) and quantity (mass deposition) of Ni-Co-Fe-Zn alloy from EMIC/EG solution.

II. EXPERIMENTAL

All chemicals used were purchased from Merck (Merck KGaA, Darmstadt, Germany). The electrodeposition of Ni-Co-Fe-Zn alloys in the presence and absence of the PPMF (9 T) were done using EMIC/EG mixed solvent, which consists of 0.25 M $NiCl_2{\cdot}6H_2O$, 0.25 M $CoCl_2{\cdot}6H_2O$, 0.25 M $FeCl_2{\cdot}4H_2O$, and 0.25 M $ZnCl_2$, which were mixed with EMIC in the glove box at 0.1 ppm oxygen and 0.2 ppm moisture. The volume ratio of EG to EMIC was 5:1 and was free from additives such as levellers and brighteners. The electrolyte was kept at room temperature, and the pH was adjusted to 4 with hydrochloric acid. The experiment for voltammetry and chronoamperometry was done in a Teflon (Titian Teraju (M) Sdn. Bhd., Kuala Lumpur, Malaysia) cell at room temperature at various potentials (–1.10 and –1.30 V) using a three-electrode setup with a Versa STAT3 PAR (Princeton Applied Research, Oak Ridge, TN) instrument. The electrodeposition setup was the same as in our previous work.[18] The SCE and platinum wire were the reference and counter electrodes, respectively. Copper plates (0.01 × 1 × 1 cm) were used as working electrodes. Each was electrochemically polished and activated by immersion into mixed acids (vol pct: HCl 30 pct-H_2SO_4 10 pct-HNO_3 5 pct-CrO_3 3 pct) for a few seconds and then rinsed with double distilled water. The electrodeposition was operated in quiescence solution with the presence and absence of PPMF (9 T). The electrochemical behavior of Ni-Co-Fe-Zn was also investigated by cyclic voltammetry (CV), where the concentration of each element was adjusted to 0.01 M for each electrolyte. The cyclic voltammograms were performed at various scan rates (1 to 20 mV/s) with the absence and in the presence of PPMF (9 T). Both chronoamperometric and CV techniques were used to study the magnetic field effect on the reduction currents. To the best of the author's knowledge, the electrodeposition of Ni-Co-Fe-Zn alloy in the presence of magnetic field in ionic liquids was not reported previously.

The topography of the deposited layers was investigated using atomic force microscopy (AFM PS 3000-NS3a, Digital Instruments, Santa Barbara, CA). The mass of electrodeposition was determined by the mass difference of the bare and coated Cu plates. A scanning electron microscope (an SEM-FEI Quanta 200F, FEI Company, Hillsboro, OR) was used to capture images of the surface morphology of the electrodeposited samples, and it included energy dispersive X-ray (EDX) analysis using energy dispersive system INCA energy 400.

III. RESULTS AND DISCUSSON

A. *CV/Chronoamperometry*

Figure 2 shows the voltammetry for the reduction currents at scan rates from 1 to 20 mV s^{-1} to determine the reduction currents for the deposition of Ni-Co-Fe-Zn alloy. Voltammograms were performed from a mixed EMIC/EG as the solvent (0.01 M of each metal) with the absence and presence of a PPMF. Regardless of the presence of the magnetic field, the diffusion-controlled currents J_1 can be written as in Eq. [1]:

$$J_1 = (2.69 \times 10^5) n^{3/2} A D^{1/2} v^{1/2} C \qquad [1]$$

where A is the area (cm^2), D is the diffusion coefficient (cm^2 s^{-1}), C is the concentration of reduction species (mol cm^{-3}), v is the scan rate (V s^{-1}), and n is the number of electrons transferred in the electrochemical reaction.

Figure 2(a) shows the reduction behavior of Ni-Co-Fe-Zn alloys at various scan rates (1 to 20 mV s^{-1}) from EMIC/EG electrolyte. It can be seen that the reduction currents are increased when the magnetic field was applied. The reduction currents were increased because of the increase in scan rates (Figure 2(a)), which is given in Eq. [1].

From the results in Figure 2(a), the relation of current i *vs* square root of scan rates $v^{1/2}$ was plotted in Figure 2(b). The increase of the currents at a specified potential is not proportional to the square root of scan rate; hence, the reduction of Ni-Co-Fe-Zn alloy is not entirely diffusion controlled. Therefore, the diffusion coefficient and kinetic constant of the reduction cannot be determined using the Gokhshtein equation from the intercept of nonlinear curves in Figure 2(b).[19] However, the currents were increased with the presence of the PPMF compared to those without the PPMF.

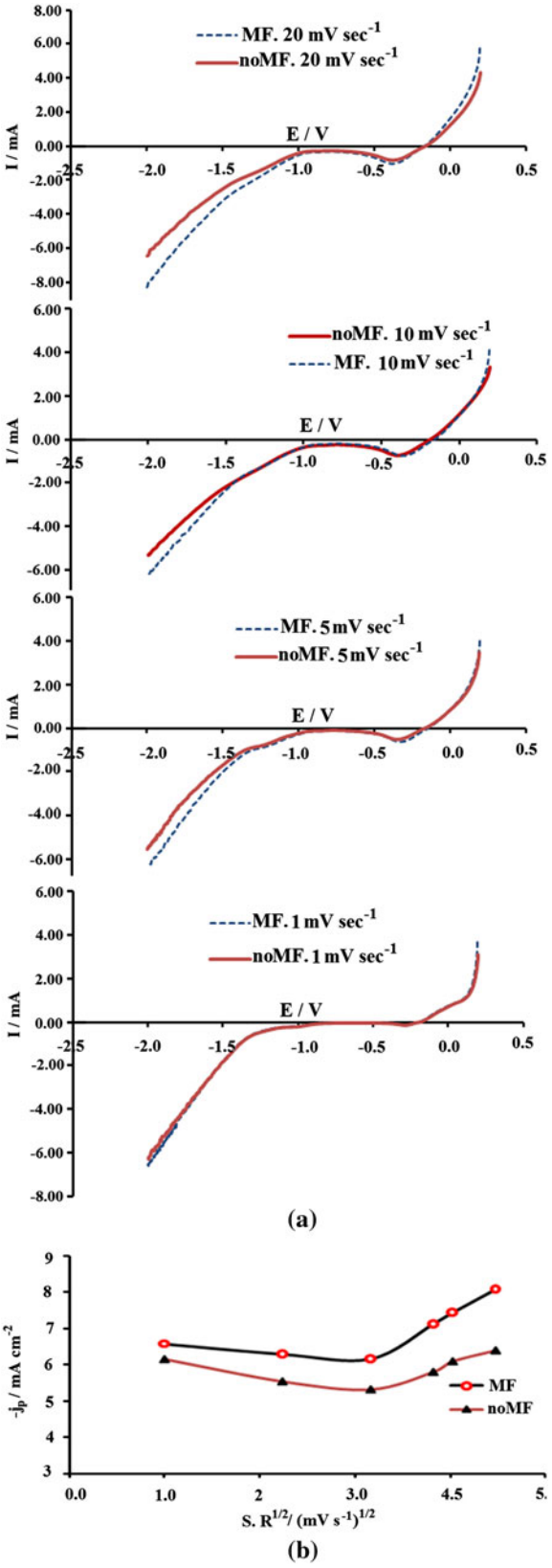

Fig. 2—(*a*) Voltammograms of Ni-Co-Fe-Zn alloys from EMIC/EG solution at various scan rates (1 to 20 mV s^{-1}) in the presence and absence of the PPMF (9 T). Concentration of each element in solution was 0.01 M during the process. (*b*) Plot of j_p *vs* $SR^{1/2}$ taken at currents at –2 V *vs* SCE from the voltammograms in (a).

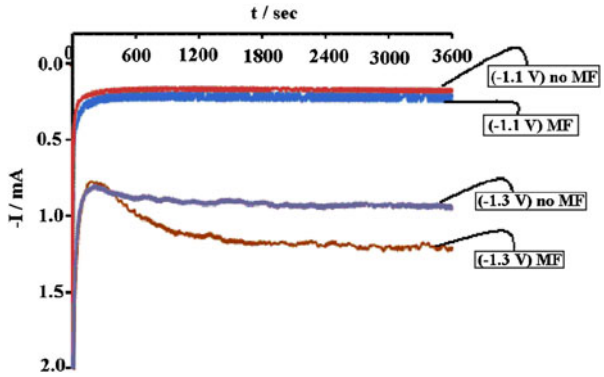

Fig. 3—Chronoamperometry of Ni-Co-Fe-Zn alloys in the presence and absence of the PPMF (9 T) at constant applied potentials (–1.10 and –1.30 V) from EMIC/EG bath. Current density values were enhanced with PPMF at the same potential.

Chronoamperometry was also used to investigate the electrodeposition of the Ni-Co-Fe-Zn alloys in the presence and absence of a PPMF (9 T) from EMIC/EG electrolyte, as shown in Figure 3. At the same applied potential, the current density was increased with the presence of the PPMF. The effect of the magnetic field on the electrodeposition of metal ions was also discussed in our previous works.[18,20] This effect is due to the normal diffusion layer thickness δ_0 diminished to a narrower diffusion layer of δ_D, when the magnetic flux B was aligned parallel to the cathode surface, although the electrodeposition of the Ni-Co-Fe-Zn alloy is not entirely a diffusion-controlled reaction. Therefore, the MHD effect (largely caused by the Lorentz force) reduces the diffusion layer thickness, thus increasing the mass transport to the electrode surface.

The chronoamperometric technique was used to characterize the mechanism of the nucleation process for the electrodeposition of Ni-Co-Fe-Zn alloys from EMIC/EG solvent in the presence and absence of a PPMF. Potentiostatic current-transient curves are shown for applied potentials of –1.10 and –1.30 V in Figure 3. According to Figure 3, the absolute value of the *I-t* transient has a normal dependency on the applied potential. It can be shown that the critical time for nucleation and growth process for the electrodeposition of Ni-Co-Fe-Zn alloys is a poor diffusion-controlled process, which will be described later. The surface coverage (θ) for nucleation can be increased by increasing the current density.[21] For long-time process, the current transient is given by

$$I_t = \frac{nAFD^{1/2}\sum C^{\infty}}{\pi^{1/2}t^{1/2}} \qquad [2]$$

where A is the area of electrode, D the diffusion coefficient, C^{∞} the bulk concentration of ions, t the time of electrodeposition process, and n the number of electrons.The nondimensional relation of $I^2/I_m^2 vst/t_m$ was plotted from the maximum I_m and t_m in the *I-t* transients during the electrodeposition process. Nucleation and growth propagation during electrodeposition can

be described from the *I-t* transients in Figure 3. However, the rate of growth is a function of electroactive species, current density, double layer, and viscosity of bulk electrolyte. The nucleation process was described by Scharifker and Hills[22] through the theory of nondimensional transients, *i.e.,* instantaneous (Eq. [3]) and progressive (Eq. [4]). The slow growth of nucleation on a small number of activation sites during the initial time of the process can be described by the instantaneous nucleation mechanism. However, progressive nucleation takes place when the rate of new nuclei formation continues over longer periods of time and the fast growth of nuclei occurs on many active sites. Figure 4 shows the typical plots together with theoretical curves from a modified Scharifker equation[22] for the instantaneous and progressive nucleation for the Ni-Co-Fe-Zn alloy at the different applied potentials. The chronoamperometric curves of the instantaneous and progressive nucleation diagrams were calculated from Eqs. [3] and [4], respectively (Figure 4).

$$\left(\frac{I(t)}{I_{\max}}\right)^2 = \frac{1.9542}{t/t_{\max}}\left\{1-\exp\left[-1.2564\left(\frac{t}{t_{\max}}\right)\right]\right\}^2 \quad [3]$$

$$\left(\frac{I(t)}{I_{\max}}\right)^2 = \frac{1.2254}{t/t_{\max}}\left\{1-\exp\left[-2.3367\left(\frac{t}{t_{\max}}\right)^2\right]\right\}^2 \quad [4]$$

where the $I_{\max}$ and $t_{\max}$ corresponds to the maximum peak current of the chronoamperometric curves and the time taken to reach the peak current, respectively. The diagrams (Figure 4) manifest that the electrodeposition of Ni-Co-Fe-Zn alloy is closer toward progressive nucleation taking into account the eventual overlap of diffusion zones.[23] According to Gunawardena *et al.,*[19,23] in the relation *I vs t*, at very short time frame ($N_0 t \to 0$), progressive nucleation (AN_0) can be defined by the following Eqs. [5–8]:

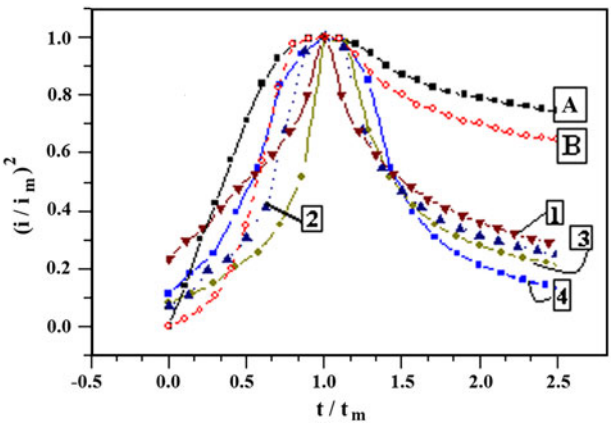

Fig. 4—The $(i/i_m)^2$ *vs* t/t_m curves for deposition of the Ni-Co-Fe-Zn alloys from EMIC/EG solution at different current densities in the absence and presence of a PPMF: (*a*) instantaneous, (*b*) progressive, and the electrodeposited layers: (1) at –1.10 V (without PPMF), (2) at –1.10 V (with PPMF), (3) at –1.30 V (without PPMF), and (4) at –1.30 V (with PPMF) *vs* SCE.

$$i(t) = \frac{2zFAN_0\pi(2DC)^{3/2}M^{1/2}t^{3/2}}{3\rho^{1/2}} \quad [5]$$

where C is the bulk concentration of species, D the diffusion coefficient from the deposition transient, zF the molar charge of electrodepositing species, A the nucleation rate constant, $i_{\max}$ the current maximum at critical time ($t_{\max}$), and the density of the electrodeposited layer (ρ) for alloys is a function of alloy equivalent weight (M):

$$M = \frac{1}{\sum \frac{n_i f_i}{A_i}} \quad [6]$$

where n_i is the valence of the alloy element i, f_i is the mass fraction of the alloy element i, and A_i is the atomic mass of element i. The diffusion coefficient can be calculated when the current maximum occurs at a time

$$t_m = \left(\frac{4.6733}{AN_0\pi K' D}\right)^{1/2} \quad [7]$$

With a maximum current density,

$$i_m = 0.4615zFD^{3/4}C(AN_0K')^{1/4} \quad [8]$$

where the $K' = \frac{4}{3}\left(\frac{8\pi CM}{\rho}\right)^2$, the product of $i_m^2 t_m$ yields

$$i_m^2 t_m = 0.2598(zFC)^2 D \quad [9]$$

The diffusion coefficient can be determined from the product of $i_m^2 t_m$ (Eq. [9]), which is independent of the nucleation and growth rate.[24] As discussed earlier, the diffusion coefficient cannot be determined from CV for Ni-Co-Fe-Zn alloys in the EMIC/EG because of the nonlinear plot of *i vs* square root of scan rates (Figure 2(b)).

Table I shows that the number of nucleation sites is increased due to the increase of applied potential (from –1.1 to –1.3 V) and applied PPMF. The falling portion of the *i-t* transient (Figure 3) can be analyzed to study the initial transient stages. The electrodeposition of Ni-Co-Fe Zn alloy in EMIC/EG solvent is confirmed as progressive nucleation by the *i vs* $t^{3/2}$ plot, which is shown in Figure 5(b). However, the *i vs* $t^{1/2}$ plots (instantaneous nucleation) in Figure 5(a) have poor linearity compared to the *i vs* $t^{3/2}$ plots (progressive nucleation) in Figure 5(b).

The slope of plots (*i vs* $t^{3/2}$, Figure 5(b)) from electrodeposition for a short time frame was studied by Origin software and from the slope of plots (Figure 5(b)); the nucleation number AN_0[18,24,25] is tabulated in Table I, where these results have good agreement with those calculated from Eq. [8]. Subsequently, it was found that the nucleation sites can be increased by both the increase of applied potential and with the presence of magnetic field. Notably, the electrodeposition of Ni-Co-Fe-Zn alloys did not occur on the electrode surface at higher potentials than –1.5 V due to the decomposition of the solvent.

Table I. Data on Progressive Nucleation Sites and Cathode Efficiency of Electrodeposited Ni-Co-Fe-Zn Layers with and without PPMF

	Electrodeposited Ni-Co-Fe-Zn Alloys			
Applied Potential	(–1.1 V) MF	(–1.1 V) No MF	(–1.3 V) MF	(–1.3 V) No MF
Progressive nucleation sites, AN_0 ($\times 10^{-6}$ cm^{-2} s^{-1})	1.276	0.843	4.984	2.392
Mass efficiency pct (PPMF)	30.25	—	68.47	—
Mass efficiency pct (no PPMF)	—	21.71	—	63.54

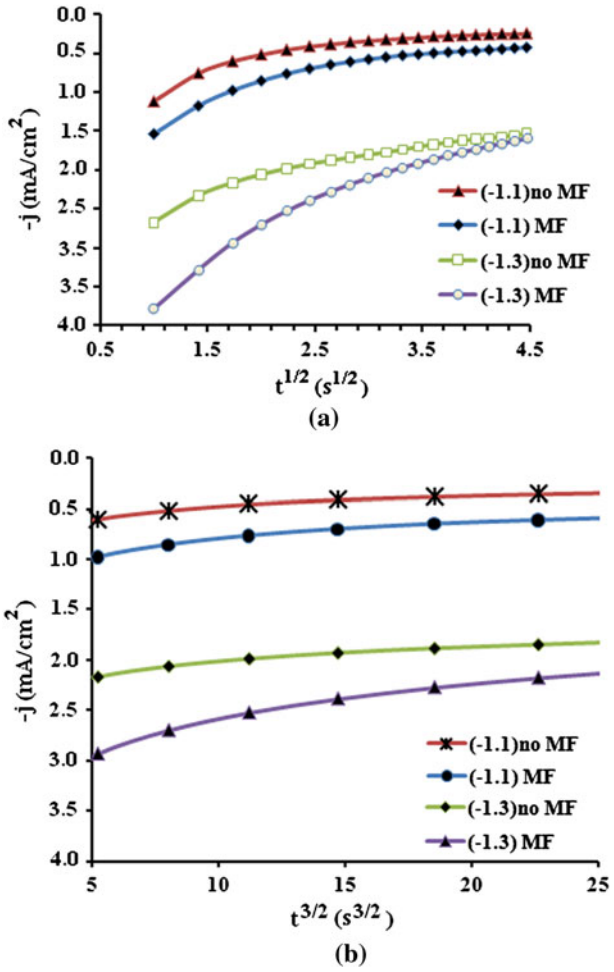

Fig. 5—Plots of (*a*) *i vs* $t^{1/2}$ and (*b*) *i vs* $t^{3/2}$ from initial transients in Fig. 3 for the Ni-Co-Fe-Zn alloy deposition to show the instantaneous and progressive nucleation mechanisms, respectively.

B. *Mass Electrodeposition*

Figure 6 shows the massogram of deposited Ni-Co-Fe-Zn alloy, which shows that the mass of electrodeposition is augmented by both the increase of applied potential (–1.1 to –1.3 V) and using the magnetic field from the EMIC/EG solvent. The role of PPMF in increasing the reduction currents was described in Section A and previous works.[18,20,26,27] It can be seen from Figure 6 that the mass of electrodeposition increases with the increase of applied potential, and the increase became slightly larger with the presence of the PPMF. With the presence of the PPMF, the

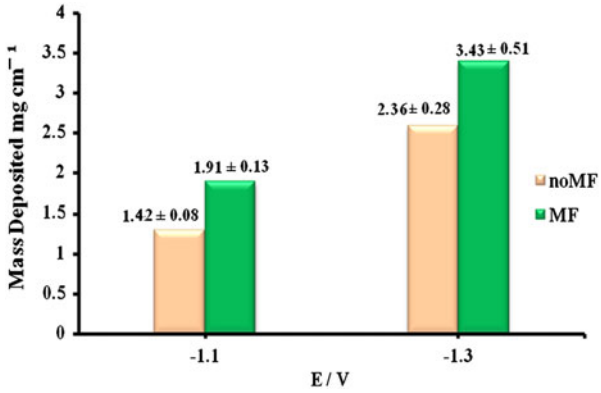

Fig. 6—Mass of deposited Ni-Co-Fe-Zn alloys is shown and increases with the increase in deposition potential with the presence and absence of the PPMF from EMIC/EG solvent.

interaction between the Lorentz force (F_L) and current density (J) will be more pronounced with the increase in applied potential; hence, the electrodeposition can be increased compared to the lower potentials. The mass deposition results were analyzed by the standard deviation equation[28] to determine errors, while the repetition of electrodepositions was performed at least 3 times.

The cathode mass efficiency is tabulated in Table I. The cathode mass efficiency is increased with the presence of the PPMF and the enhancement of current density is due to the increase in applied potential. The increase of mass efficiency could be affirmed by the increase of nucleation sites when the applied potential was increased from –1.1 to –1.3 V. Contrarily, it was reported by our previous work[18] that the efficiency of electrodeposition was reduced with the increase of applied potential (–1.1 to –1.3 V) for Ni-Co-Fe-Zn alloys due to the hydrogen evolution reduction (HER) in aqueous solution. Ispas[29] and Dolati *et al.*[30] reported that the nucleation sites can be increased to initiate more surface coverage (θ) of the nuclei during the electrodeposition process with the increase of applied potential and the presence of the PPMF. Those deductions also agree with our results. Worth noting is the fact that the Ni-Co-Fe-Zn alloys were not deposited on the cathode surface at applied potential ≥–1.5 V. This is because the decomposition of mixture EMIC/EG occurred on the electrode surface at applied potential ≥–1.5 V. In this case, the smaller potential window for electrodeposition process is a clear disadvantage for the EMIC/EG solvent.

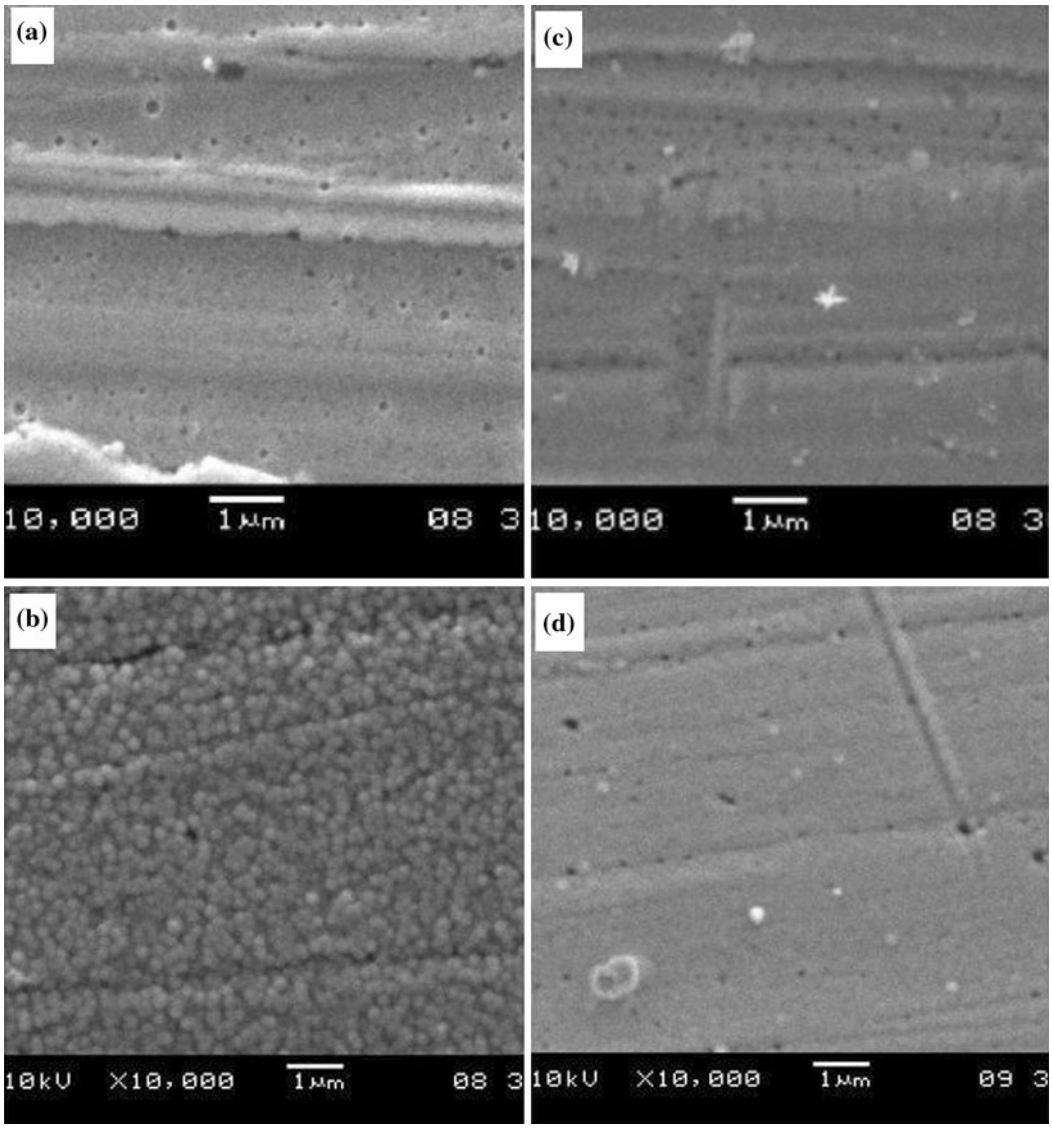

Fig. 7—SEM micrograph (magnification 10,000 times) of Ni-Co-Fe-Zn electrodeposition without PPMF: (*a*) –1.10 V and (*b*) –1.30; and with PPMF (9 T): (*c*) –1.10 V, (*d*) –1.30 V *vs* SCE.

C. *Scanning Electron Microscopy/EDX Analysis*

Scanning electron microscopy (SEM) was used to investigate the surface morphology of the Ni-Co-Fe-Zn alloy layers, which were obtained from a mixture of EMIC/EG electrolytes with a magnification of 10,000 times at 10 kV. The SEM images (Figures 7(a) and (c) and Figures 7(b) and (d)) are layers that were electrodeposited at –1.10 and –1.30 V, respectively. The images in Figures 7(c) and (d) are layers electrodeposited with the presence of the PPMF (9 T). The EDX spectrums in Figures 8(a) through (d) correspond to the SEM images in Figures 7(a) through (d). Figure 7(b) shows the rounded grain shapes obtained from electrodeposition with the absence of the PPMF; on the other hand, Figure 7(d) shows a more uniform electrodeposited surface due to the applied magnetic field. It can be deduced that the PPMF affected the arraying of atoms during electrodeposition. Worthy of note is the fact that the morphologies of Ni-Co-Fe-Zn alloy layers electrodeposited from aqueous[19] and EMIC/EG are totally different. Furthermore, the electrodeposition of the Ni-Co-Fe-Zn alloy surface from EMIC/EG is more uniform compared to the electrodeposited surface from aqueous solution with the same conditions, *i.e.*, temperature, applied potential, and presence and absence of a PPMF.

Anomalous behavior was also investigated with different current densities by other researchers.[7,31] Lodhi and co-workers[7] found that with the presence of the less noble metals (*i.e.*, Fe, Zn), the anomalous behavior appears with the increase of current density during the codeposition of metals. Interestingly, two different types of electrodeposition can be illustrated in Figure 8. The normal electrodeposition of Ni-Co-Fe-Zn alloy can be seen at potential –1.1 V, whereas the codeposition at –1.3 V led to anomalous behavior.

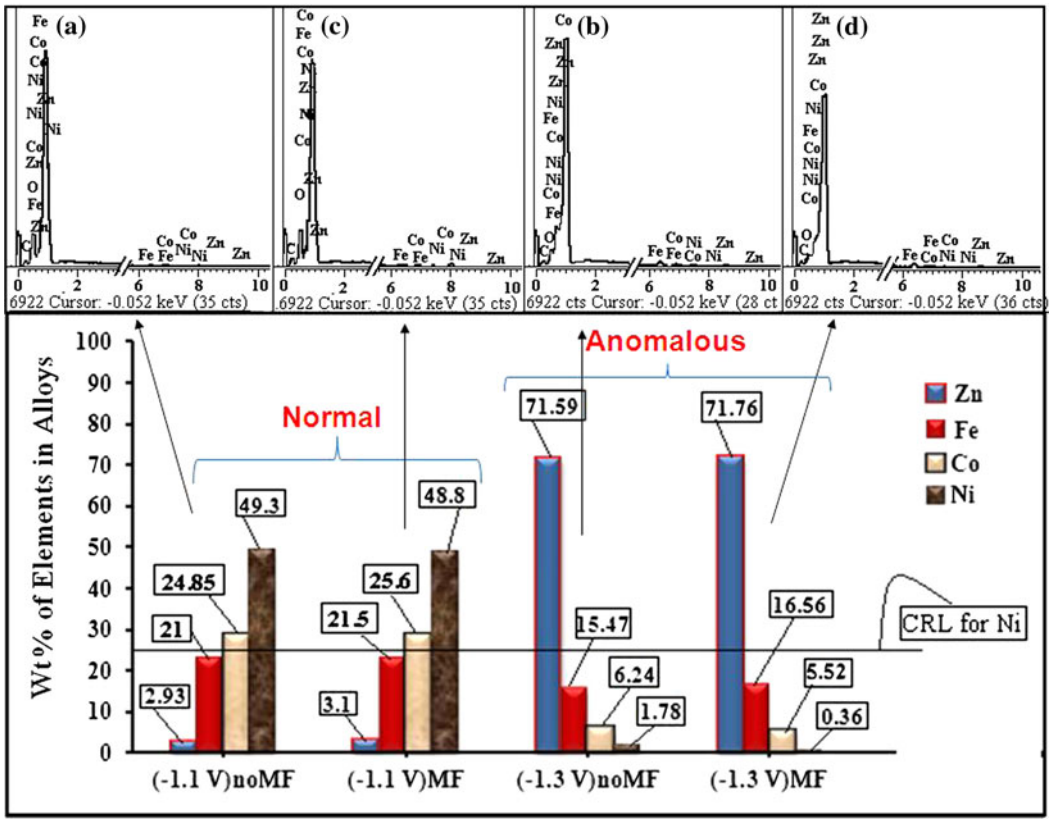

Fig. 8—EDX spectrum (top) and results (bottom) of the weight percentages of elements in Ni-Co-Fe-Zn alloys electrodeposited from EMIC/EG solvent at potentials of –1.10 V and –1.30 V with the absence and presence of the PPMF (9 T), together with the total percentages of the elements in all four electrodeposited alloys. The CRL line of Ni is 25 pct.

There seems to be an abrupt change that occurred from deposition potential of –1.1 to –1.3 V. This phenomenon is still unclear, but it can be suggested that the UPD of the less noble metals with the presence of the more noble metals could be one of the causes of this behavior.

The elemental composition of the galvanostatically deposited alloys was determined by EDX and illustrated in Figure 8. The composition reference line (CRL) was used to show the normal and anomalous behaviors of co-electrodeposition alloys. The CRL of Ni is defined as[18]

$$\mathrm{CRL} = \frac{c(\mathrm{Ni}^{2+})}{\left[c(\mathrm{Ni}^{2+} + \mathrm{Co}^{2+} + \mathrm{Fe}^{2+} + \mathrm{Zn}^{2+})\right]} \times 100 \quad [10]$$

where c is the concentration of each ion (*e.g.*, c(Ni) is the concentration of Ni^{2+} in the electrolyte).

The CRL for Ni (25 pct) is drawn in Figure 8(b). It shows that the Ni composition in the electrodeposition layers is higher than the CRL for deposition at –1.1 V. On the other hand, the electrodeposition of Ni falls below the CRL with the increase in the deposition potential to –1.3 V. With respect to the HSM mechanism, it may not only occur in aqueous solutions, but could also be due to the presence of the water molecules from the hydrated metal salts in the mixed EMIC/EG solvent. Consequently, it was found that the co-electrodepositions are strongly dependent on the applied potential value. Notably, the decomposition of EMIC/EG during the electrodeposition can be illustrated through the EDX graphs in Figure 8(a), where the presence of carbon on the deposited surface is due to the decomposition of EMIC/EG.

D. *AFM Analysis*

Atomic force microscopy (AFM) was used to determine the surface roughness of the Ni-Co-Fe-Zn alloys. Figure 9 presents the three-dimensional (3-D) AFM images of the Ni-Co-Fe-Zn surface electrodeposited from EMIC/EG with the presence and absence of the PPMF (9 T). The 3-D AFM images were obtained from a scanning surface of 5 × 5 μm. The images in Figures 9(a) and (c) were obtained from electrodeposition of the Ni-Co-Fe-Zn alloys at –1.10 V, while those in Figures 9(b) and (d) were obtained from electrodeposition at –1.30 V from the mixed EMIC/EG solvent.

In Figure 9, the 3-D AFM images of the alloy electrodeposition with the presence of the PPMF are on the right, while the 3-D AFM images of the alloy electrodeposition with the absence of the PPMF are on the left. The roughness of deposited layers was determined from the AFM results. The surface roughness of an $L \times L$ area (R_a (L)) could be calculated by using the root-mean-square value defined as[32]

$$R_a(L) = \sqrt{\sum_i^n \frac{(\bar{h} - h_i)^2}{n}} \quad [11]$$

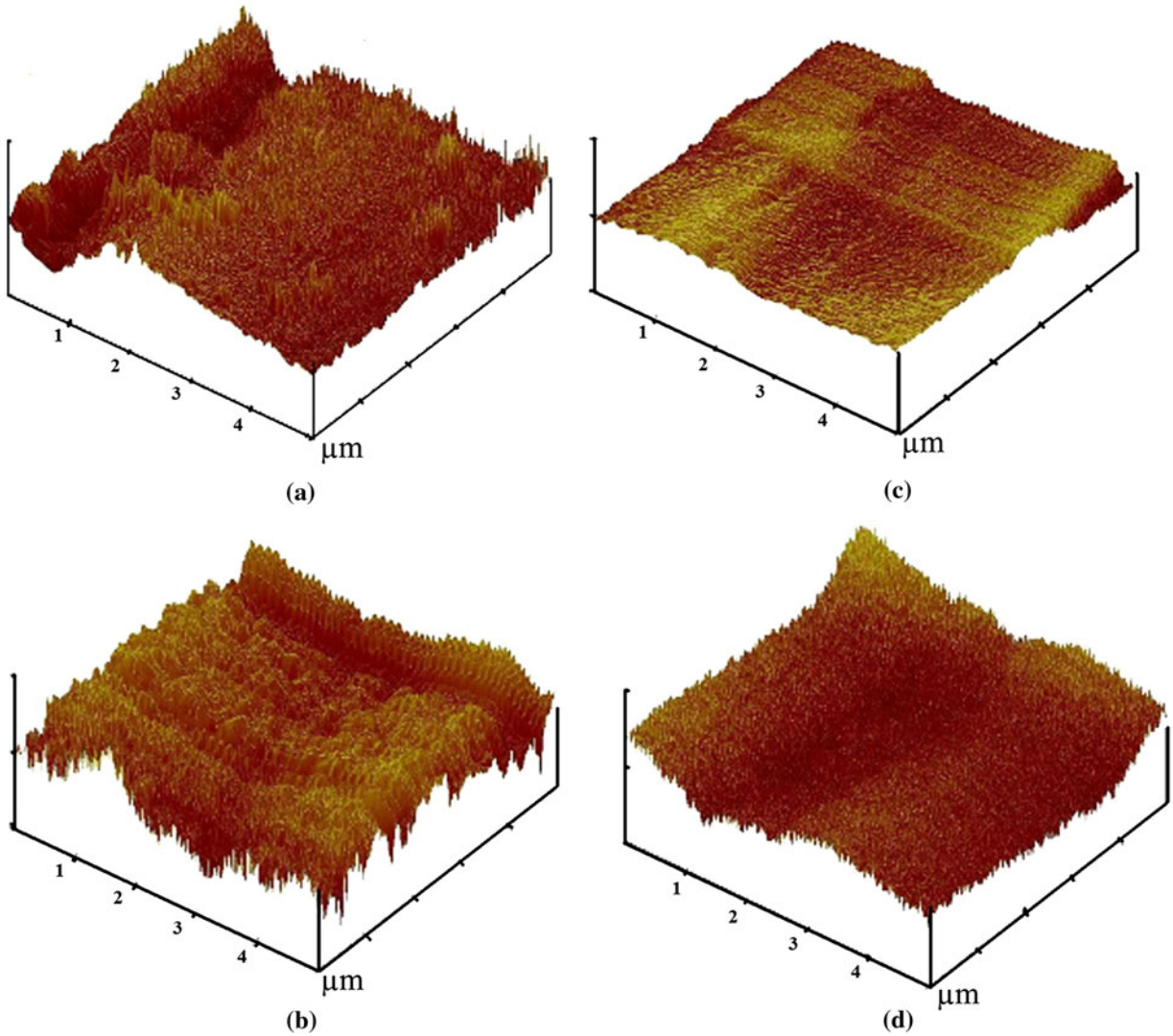

Fig. 9—AFM images of Ni-Co-Fe-Zn alloy surface electrodeposited in the absence of PPMF: (*a*) –1.10 V and (*b*) –1.30 V; and with PPMF (9 T): (*c*) –1.10 V and (*d*) –1.30 V *vs* SCE.

where n is the number of points measured across a surface $L \times L$, $\bar{h}$ is the average height, and h_i is the height of each point. From the AFM results, it was found that the surface roughness of the electrodeposited layers with the presence of the PPMF is reduced compared to that with the absence of the PPMF at the same deposition potentials. At a deposition potential of –1.10 V, the roughness factor was reduced from 33.56 nm (without PPMF) to 11.58 nm (with PPMF), while at a depositon potential of –1.30 V, the roughness factor was reduced from 45.28 nm (without PPMF) to 39.44 nm (with PPMF). These results show that the roughness of electrodeposited layers from EMIC/EG is lower than that with layers electrodeposited from aqueous solution.[18] Koza *et al.*[33] investigated the influence of PPMF on the dendrites and branches during electrodeposition, but the smoothness effect of the magnetic field on the electrodeposition process is still unclear. Nikolić *et al.*[18] suggested that the PPMF has a smoothness effect in the double layer vicinity of the electrodeposited surface where the arraying of ions could take place during the electrodeposition process.

IV. CONCLUSIONS

Potentiostatic electrodepositions of Ni-Co-Fe-Zn alloy at potentials –1.10 and –1.30 V *vs* SCE gave normal and anomalous electrodepositions. The normal deposition was observed at –1.10 V, whereas the anomalous deposition was observed at –1.30 V, where both occurred with the absence and presence of a PPMF (9 T). It can be concluded that the normal electrodeposition of Ni-Co-Fe-Zn alloy layers from EMIC/EG can be controlled by lower applied potentials. The mass efficiency percent increased from 21.71 (without PPMF) to 30.25 (with PPMF) at –1.10 V and from 63.54 (without PPMF) to 68.47 (with PPMF) at –1.30 V. It was found that the electrodeposition is not an entirely

diffusion-controlled process. From the linear plots of i *vs* $t^{3/2}$ and $\left(I^2/I^2_{\max}\right)$*vs* $\left(t/t_{\max}\right)$, it can be deduced that the electrodeposition takes place by a progressive nucleation mechanism.

ACKNOWLEDGMENTS

We thank the University of Malaya for the financial support provided by University Research Grant No. PS 350/2009C and UMCiL Grant Nos. TA009/2008A and TA007/2009A.

REFERENCES

1. A. Brenner: *Electrodeposition of Alloys. Principles and Practice*, Academic Press, New York, NY, 1963, vols. 1 and 2.
2. L. Péter, A. Csik, K. Vad, E. Tóth-Kádár, A. Pekker, and G. Molnár: *Electrochim. Acta*, 2010, vol. 55 (16), pp. 4734–41.
3. C.K. Chung and W.T. Chang: *Thin. Sol. Film*, 2009, vol. 517 (17), pp. 4800–04.
4. J.A. Koza, M. Uhlemann, A. Gebert, and L. Schultz: *Electrochim. Acta*, 2008, vol. 53 (16), pp. 5344–53.
5. H. Dahms and I.M. Caroll: *J. Electrochem. Soc*., 1965, vol. 112 (8), pp. 771–75.
6. Z.F. Lodhi, F.D. Tichelaar, C. Kwakernaak, J.M.C. Mol, H. Terryn, and J.H.W.A. de Wit: *Surf. Coat. Technol*., 2008, vol. 202 (12), pp. 2755–64.
7. Z.F. Lodhi, J.M.C. Mol, W.J. Hamer, H.A. Terryn, and J.H.W. de Wit: *Electrochim. Acta*, 2007, vol. 52 (17), pp. 5444–52.
8. P.-Y. Chen and I.-W. Sun: *Electrochim. Acta*, 2001, vol. 46, pp. 1169–77.
9. M.J. Nicol and H.I. Philip: *J. Electroanal. Chem*., 1976, vol. 70 (2), pp. 233–37.
10. S. Swathirajan: *J. Electroanal. Chem*., 1987, vol. 221 (1–2), pp. 211–28.
11. Z.F. Lodhi, J.M.C. Mol, A. Hovestad, H. Terryn, and J.H.W. de Wit: *Surf. Coat. Tech*., 2007, vol. 202 (1), pp. 84–90.
12. A. Cojocaru, S. Costovici, L. Anicai, and T. Vişan: *Met. Int*., 2009, vol. 14 (11), pp. 38–46.
13. L. Xu, J. Du, S. Ge, N. He, and S. Li: *J. Appl. Electrochem*., 2009, vol. 39 (5), pp. 713–17.
14. F. Zhao, F. Xiao, and B. Zeng: *Electrochem. Comm*., 2010, vol. 12 (1), pp. 168–71.
15. S.-P. Gou and I.-W. Sun: *Electrochim. Acta*, 2008, vol. 53 (5), pp. 2538–44.
16. N. Koura, Y. Suzuki, Y. Idemoto, T. Kato, and F. Matsumoto: *Surf. Coat. Technol*., 2003, vols. 169–170, pp. 120–23.
17. A.P. Abbott, K. El Taib, K.S. Ryder, and E.L. Smith: *Trans. Inst. Met. Finish*., 2008, vol. 86 (4), pp. 234–40.
18. M. Ebadi, W.J. Basirun, Y. Alias, and M.R. Mahmoudian: *Chem. Central. J*., 2010, vol. 4 (1), p. 14.
19. M. Rezaei, M. Ghorbani, and A. Dolati: *Electrochim. Acta*, 2010, vol. 56, pp. 483–90.
20. M. Ebadi, W.J. Basirun, and Y. Alias: *J. Chem. Sci*., 2010, vol. 122 (2), pp. 279–85.
21. Y. Zhuang: Ph.D. Thesis, Louisiana State University, Baton Rouge, LA, 1995.
22. B.R. Scharifker: *J. Electroanal. Chem*., 1998, vol. 458 (1–2), pp. 253–55.
23. A.B. Soto, E.M. Arce, M. Palomar-Pardavé, and I. González: *Electrochim. Acta*, 1996, vol. 41 (16), pp. 2647–55.
24. L. Mentar, M.R. Khelladi, A. Azizi, and A. Kahoul: *Mater. Lett*., 2010, vol. 64 (21), pp. 2403–06.
25. A. Dolati, M. Sababi, E. Nouri, and M. Ghorbani: *Mater. Chem. Phys*., 2007, vol. 102 (2–3), pp. 118–24.
26. M. Ebadi, W.J. Basirun, and Y. Alias: *Asian J. Chem*., 2009, vol. 21 (8), pp. 6343–53.
27. M. Ebadi, W.J. Basirun, and Y. Alias: *Asian J. Chem*., 2009, vol. 21 (9), pp. 7354–62.
28. J.N. Miller and J.C. Miller: *Statistics and Chemometrics for Analytical Chemistry*, 5th ed., Great Britain by Ashford Colour Press, Gosport, Hants, 2005.
29. A. Ispas: Ph.D. Thesis, Technical University of Dresden, Germany, 2007.
30. A. Dolati, A. Afshar, and H. Ghasemi: *Mater. Chem. Phys*., 2005, vol. 94 (1), pp. 23–28.
31. Y.M.F. Marikar and K.I. Vasu: *Electro. Surf. Treat*., 1974, vol. 2 (4), pp. 281–94.
32. N.D. Nikolić, H. Wang, C. Guerrero, E.V. Ponizovskaya, G. Pan, and N. Garcia: *J Electrochem. Soc*., 2004, vol. 151 (9), pp. C577–C584.
33. J.A. Koza, M. Uhlemann, C. Mickel, A. Gebert, and L. Schultz: *J. Mag. Mag. Mater*., 2009, vol. 321 (14), pp. 2265–68.